Available online at www.sciencedirect.com
SCIENCE DIRECT
Catalysis Today 110 (2005) 239–246
CATALYSIS TODAY
www.elsevier.com/locate/cattod

Changes in states of substituted iron in microporous (MFI analogue) and mesoporous (MCM-41) hosts exposed to redox conditions

Károly Lázár [a,*], Ágnes Szegedi [b], Gabriella Pál-Borbély [b], A.N. Kotasthane [c], Pál Fejes [d]

[a] *Institute of Isotopes, CRC, HAS, P.O. Box 77, Budapest H-1525, Hungary*
[b] *Institute of Surface Chemistry and Catalysis, CRC, HAS, P.O. Box 17, Budapest H-1525, Hungary*
[c] *United Catalysts Ltd., 391340 Nandesari, India*
[d] *Department of Applied and Environmental Chemistry, University of Szeged, Szeged H-6720, Hungary*

Available online 20 October 2005

Abstract

Iron was incorporated into microporous MFI analogue (ZSM-5, Si/Fe ~ 200 and FER, Si/Fe = 16) and mesoporous MCM-41 hosts of different preparations (Si/Fe ~ 100 and 20, respectively). Samples were characterized by in situ Mössbauer spectroscopy under various conditions. Framework (FW) and extra-framework (EFW) sites can be distinguished in relation with strict three-dimensional (3D) crystallinity of the structure. In addition, in the microporous ZSM-5 system occurrence of Fe^{4+} oxidation state is hypothesized and reversible $Fe^{4+} \leftrightarrow Fe^{3+}$ transformation is presumed for a minor portion of iron. Spectra of Fe-FER are interpreted in terms of dynamic formation and decomposition of Fe_{FW}–O–Fe_{EFW} dinuclear centres. In the mesoporous systems, the partly amorphous character of the pore wall is correlated with the redox behaviour and coordination of incorporated iron; larger portion of iron may take part in $Fe^{3+} \leftrightarrow Fe^{2+}$ reversible processes and Fe^{2+} may be stabilized in distorted coordination (not appearing in microporous structures).

Keywords: Iron; Redox processes; Mössbauer spectroscopy; Porous hosts

1. Introduction

Substitution of iron is widely used to modify the original properties of porous catalyst hosts, both in micro- and mesoporous structures. Both the acidity and redox properties can be modified by inserting iron into the structure. Namely, substitution into framework (FW) sites modifies acidity, whereas iron in extra-framework (EFW) position may generate redox centres. Iron-containing microporous catalysts have important applications (to name a few: NO_x decomposition, generating alpha-oxygen for controlled oxidation, e.g. benzene to phenol, etc.) [1]. MFI-related structures are widely studied among microporous systems due to their good performance and high stability [2,3]. Mesoporous systems attract also interest—since the mesoporous host may accommodate larger molecules in the pores allowing catalytic processes for broad variety of reactions [4].

Incorporation of iron raises the aspect of stability, i.e. the position of iron and possible transformations in coordination and oxidation states occurring under catalytic conditions should be anticipated. In this regard, the crystallinity of host is of primary importance; coordination and redox properties of iron species present in strictly crystalline three-dimensional (3D) microporous systems may be distinctly different from properties of iron located in mesoporous hosts possessing partly amorphous structure in their pore walls [5].

Mössbauer spectroscopy is a devoted tool for characterizing the close neighbourhood of iron, both as for coordination and oxidation states. There exist good compilations of data as for interdependence of Mössbauer parameters (isomer shift (IS) and quadrupole splitting (QS)) with the coordination and the structure, e.g. for silicate minerals [6]. In short, increasing

* Corresponding author. Fax: +36 1 392 2584.
E-mail address: lazar@iserv.iki.kfki.hu (K. Lázár).

0920-5861/$ – see front matter © 2005 Elsevier B.V. All rights reserved.
doi:10.1016/j.cattod.2005.09.024

symmetry results in decrease of QS for high-spin Fe^{3+}, and the connection is opposite for Fe^{2+}. In correspondence, the method has successfully been applied since the early paper of Meagher et al. [7]. It was demonstrated that distinction between the FW and EFW positions is also possible, e.g. by comparing the reducibility of Fe^{3+}. Namely, FW iron is hardly reducible, whereas reduction of EFW iron is possible (e.g. in H_2 at 600 K). Further, symmetry of charge compensating cation has also influence on the charge distribution at the framework substituted ion (reflected in the QS), e.g. Bronsted acidic H^+ in the vicinity of substituted iron results in high distortion (QS ∼ 1.7–1.9 mm/s), whereas other cations of larger diameter result in less asymmetry (QS ∼ 1.2–1.4 mm/s) [8]. Other features are reflected in the spectra as well. Namely, the sole ionic incorporation can be deduced from relaxation phenomena in the spectra recorded at low temperatures [9] or structures on which alpha-oxygen may be stabilized can also be characterized by delicate measurements [10].

In the present study, properties of iron incorporated to microporous (MFI analogue) and mesoporous (MCM-41) hosts are compared, their oxidation and coordination states are analysed mostly by in situ Mössbauer spectroscopy. A special motivation in selecting the particular hosts was to compare the effect of different crystallinities of structures, to reveal in what extent are they reflected in the corresponding Mössbauer spectra.

2. Experimental

2.1. Syntheses

ZSM-5 (Si/Al = Si/Fe = 200) have been synthesized by hydrothermal way, using sodium silicate solution, colloidal silica (Ludox), sodium hydroxide, iron sulphate, aluminium oxide trihydrate and tetrapropyl-amonium bromide as template. The crystallization was performed in teflon-lined autoclave at 430 K (6–12 h). After calcination, the sodium form was converted to (NH_4^+, H^+) form by repeated ion exchange in slightly acidified 1 M NH_4NO_3 solution. The synthesis procedure is described in detail [11]. To improve the signal to noise ratio in Mössbauer spectra ^{57}Fe was used as iron source.

Fe-FER (Si/Fe = 16) was synthesized starting with acidic solution of $Fe_2(SO_4)_3$ then by adding sodium silicate solution, and addition of pyrrolidine later. The gel was autoclaved at 433 K for 48 h. After calcination at 773 K, the H^+/Na^+ form was converted to NH_4^+ form by multiple exchange with 2 M NH_4NO_3 solution. After drying, the sample was calcined at 753 K. The synthesis is described in more detail in Ref. [12].

Fe-MCM-41 samples were synthesized in two ways:

(1) A low iron-content (Si/Fe ∼ 100) sample was prepared by hydrothermal process, using ^{57}Fe isotope as iron source (in order to improve the detection of Mössbauer signal). The gross composition of the gel was—$1SiO_2$:$0.005Fe_2SO_4$:$0.2Na_2O$:$0.83Na_2SO_4$:$0.29C_{16}$TMABr:$50H_2O$. The synthesis was performed at 370 K under autogeneous pressure for 170 h. The removal of template was performed by ramping the temperature to 753 K in nitrogen stream, followed by a final calcination in air at this temperature for 1.5 h. The procedure is described in more detail in Ref. [13].
(2) Fe-MCM-41 (Si/Fe = 20) sample was prepared by a rapid method using TEOS as silica source, and the synthesis mixture was complemented with ethanol. The composition applied—1TEOS:$0.05Fe(NO_3)_3$:$0.3C_{16}$TMABr:$11NH_3 \cdot 255H_2O$:58EtOH . The gel was formed already at room temperature by adding the last component, ammonia to the solution made of the previous components. The template removal was performed in the same way as in synthesis (1). The particular feature of this synthesis is that the product mostly forms spherical particles with a diameter of 150–350 nm [14].

2.2. Mössbauer spectroscopy

In situ Mössbauer spectra were recorded in a versatile measuring cell [15]. Various treatments were applied to study the coordination of iron, i.e. evacuation, CO and hydrogen reductions. Spectra were collected in constant acceleration mode, by using $^{57}Co/Rh$ (1 GBq) source. Spectra were decomposed to Lorentzian line shape components. The isomer shift values are relative to metallic alpha-iron. The accuracy of positional data is ca. ± 0.03 mm/s. It should be reminded here that the isomer shift values depend on the temperature of measurement as well, i.e. this shift should also be taken into account when comparing the IS values of components extracted from spectra recorded at different temperatures (in a rough approximation: −0.1 mm/s for $+\Delta T$ of 100 K). Spectra were recorded subsequently, i.e. without changing the sample—several treatments were performed on the same single sample.

3. Results and discussion

3.1. Microporous samples (1) ZSM-5 (Si/Fe = Si/Al = 200)

To check the quality of the synthesis, spectra were obtained first on the product (before ion exchange with NH_4NO_3) in wide velocity range at 300 and 77 K (Fig. 1a and b). At 300 K, a broad central single line appears, which is converted to a spectrum exhibiting partial magnetic ordering upon cooling the sample to 77 K (the magnetic field corresponding the splitting of outermost lines in the 77 K spectrum is 50.6 T). The two spectra can be interpreted in terms of spin–spin and spin–lattice relaxations. The former depends on the distance of the nearest iron ions (i.e. iron-content) and does not depend on the temperature. In contrast, the second process, spin–lattice relaxation depends on the temperature [16]. At higher temperature (300 K), spins are relaxing at a faster rate, canceling the effective average magnetic field around iron. At 77 K, the spins of single isolated Fe^{3+} ions retain their direction to a period sufficient for appearance of magnetization in the spectrum (a few nanoseconds). It should also be mentioned that strong coupling (existing in dimeric, oligomeric iron species) results in dia-, and paramagnetism, the magnetic splitting

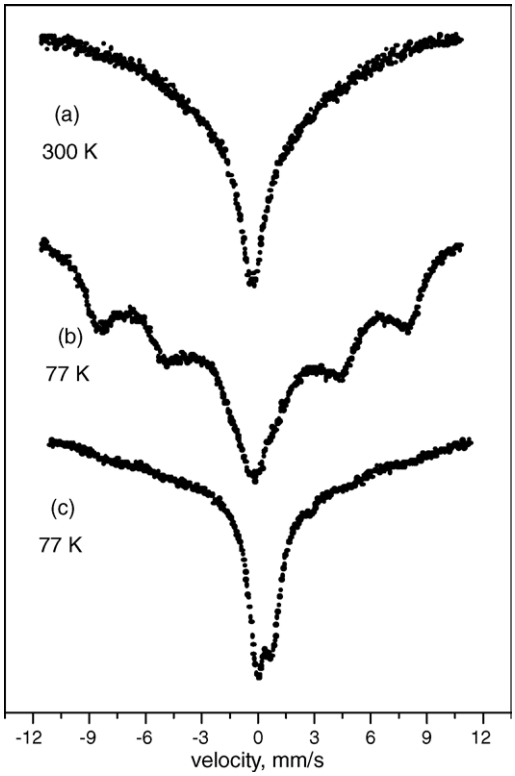

Fig. 1. Mössbauer spectra of the ZSM-5 (Si/Fe = Si/Al = 200) sample: (a) after synthesis, recorded at 300 K; (b) after synthesis, recorded at 77 K; (c) after having finished the series of treatments (shown in Fig. 2), recorded at 77 K.

originated from single ionic spins of Fe^{3+} cannot be detected [16].

Similar change in the shape of spectra has been reported for zeolites of low iron-content (for Si/Fe < 150, e.g. in Refs. [7,9]). At higher iron concentrations the spin–spin relaxation is faster—and the magnetic order does not appear even at very low temperatures (e.g. 4.2 K is not sufficiently low for Si/Fe = 19 [17]). The isomer shift value obtained for the broad central component in Fig. 1a is 0.28 mm/s, attesting for the prevalent tetrahedral, FW location of iron. Hence, the good quality of the synthesis is demonstrated; spectra of Fig. 1a and b show the dominance of separated single FW Fe^{3+} ions.

In the series of treatments evacuation was used first—this step usually removes the chemisorbed water from the vicinity of iron, enabling thereby the identification of coordination sites characteristic of the structure [8]. Hydrogen reduction was used to distinguish between the FW and EFW sites. Thereafter, N_2O was introduced at a modest temperature to restore the oxidized state. CO was introduced subsequently to the sample at room temperature to study whether reduction proceeds at 300 K. The series of spectra is shown in Fig. 2. To monitor the changes in better resolution, in situ spectra were recorded in shorter velocity range. Spectra were decomposed by fitting, the respective data are collected in Table 1. For the sample the mean centres of spectra were also determined—to obtain a rough hint on the average oxidation state of iron (isomer shift value of high spin iron ions increases monotonously with decrease of the oxidation number [18]).

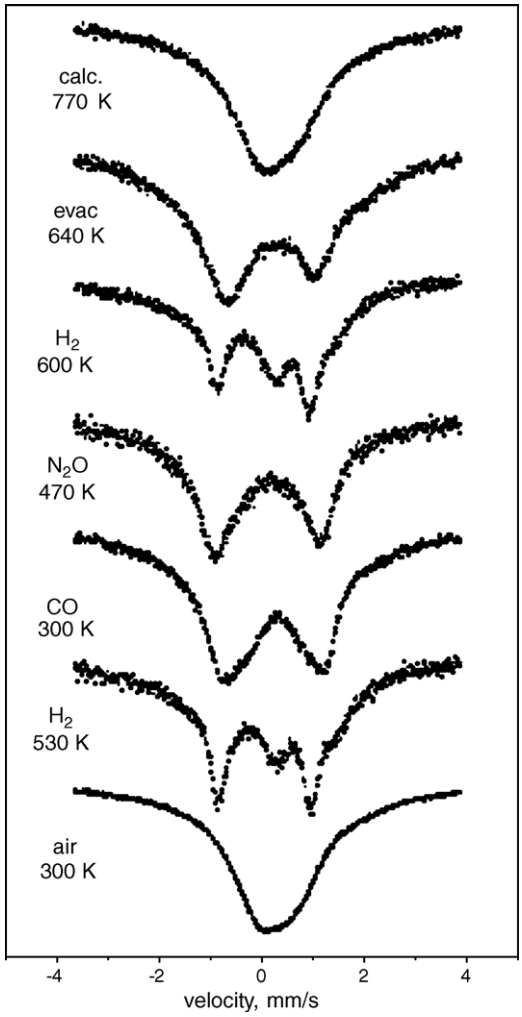

Fig. 2. Sequential in situ Mössbauer spectra recorded on the FeZSM-5 sample (Si/Fe ∼ 200) in a series of treatments (starting at the top with calcination).

The largest component in the first spectrum in Fig. 2 is similar to that shown in Fig. 1a, i.e. ion exchange does dot result in significant change, a broad featureless line is retained. However, the ex situ calcination applied at 820 K results in the removal of a minor portion of the FW iron to EFW position as reflected in the appearance of a complementing doublet. The first in situ treatment, evacuation results already in a surprising spectrum. Namely, relying on the decomposition, apart from Fe^{3+}, appearance of Fe^{4+} can be suggested with simultaneous presence of Fe^{2+}. The mean of the spectrum (IS_{av} = 0.03 mm/s) is convincing; regardless to any fitting the mean centre is close to the isomer shift of Fe^{4+} (∼ −0.1 mm/s).

The further treatment in hydrogen at 600 K results in an expected shape and spectrum decomposition. Namely, the Fe^{3+} component of high quadrupole splitting can be attributed to FW iron (for ca. in two/thirds part), and one-third is probably removed and is in EFW Fe^{2+} sites of various coordination. Surprisingly again, the Fe^{4+} state is restored by evacuation and oxidation with N_2O at 470 K for a noticeable part of iron (27% of the spectrum). Curiously, the Fe^{4+} is retained in part even in CO at ambient temperature (with 13% RI). The oxidation with N_2O at 470 K resulted in certain stabilization of Fe^{3+} as well—

Table 1
Mössbauer data obtained from selected spectra recorded after sequential treatments of FeZSM-5 sample (Si/Fe ~ 200)

Treatment/(measurement)	Compound	IS (mm/s)	IS_{av} (mm/s)	QS (mm/s)	RI (%)
As-received/calcined	Fe^{3+}	0.23	0.25	–	87
	Fe^{3+}	0.37		0.90	13
640 K/vac. (300 K)	Fe^{4+}	−0.33	0.03	1.45	49
	Fe^{3+}	0.21		1.76	37
	Fe^{2+}	0.85		2.51	14
600 K/H_2 (570 K)	Fe^{3+}	0.01	0.27	1.72	63
	Fe^{2+}	0.67		0.71	19
	Fe^{2+}	0.77		1.37	18
470 K/N_2O (470 K)	Fe^{4+}	−0.16	0.02	0.91	27
	Fe^{3+}	0.11		2.03	73
CO/300 K (300 K)	Fe^{4+}	−0.13	0.16	–	13
	Fe^{3+}	0.20		1.83	87
530 K/H_2 (530 K)	Fe^{3+}	0.08	0.24	1.82	55
	Fe^{3+}	0.15		–	28
	Fe^{2+}	0.90		1.18	17
300 K/air (300 K)	Fe^{3+}	0.19	0.26	0.68	59
	Fe^{3+}	0.36		–	41

In parentheses, the temperature of measurement is shown. IS: isomer shift, relative to metallic alpha-iron; IS_{av}: the mean isomer shift (centre of gravity of spectrum); QS: quadrupole splitting; RI: spectral contribution (relative intensity).

reduction with hydrogen in a moderate temperature 530 K restores only in part the Fe^{2+} percentage observed at the first hydrogenation at 600 K. Further, leaving the sample on air, a featureless spectrum can be recorded (bottom of Fig. 2). This sample was measured at wide velocity range at 77 K (Fig. 1c). The change is apparent, when comparing the spectrum to the state shown before treatments (Fig. 1b). By decomposition, ca. one-half of the spectral area can be assigned to the relaxing broad background, while the other one-half part appears in the doublets in the centrum. Thus, the comparison clearly shows that significant rearrangement has taken place during the series of treatments, the original single separate ionic location has been modified for ca. one-half part of the iron even at a rather dilute Si/Fe = 200 ratio.

As for the unexpected presence of Fe^{4+}, we cannot provide a proven explanation and further studies are necessary to strengthen the assumption. Reports on possible occurrence of Fe^{4+} in ZSM-5 are scarce. From experimental side an EXAFS study is published in which occurrence of Fe^{4+} is proposed in Fe-MFI [19]. In turn, from theoretical aspect, existence of mononuclear Fe^{4+} centres is hypothesized in the recent comprehensive paper of Heyden et al. by reporting on DFT calculations on the decomposition of nitrous oxide over Fe-ZSM-5 [20]. Or Yakovlev et al. presumed also the existence of Fe^{4+} in dinuclear centres at lower temperature in modeling the same process [21]. Anyhow, this component seems to be present, not only at evacuation but its contribution was restored in part by a modest temperature (470 K) oxidation with N_2O.

3.2. Microporous samples (2) Fe-FER (Si/Fe = 16)

The pore system of FER structure can be related to the MFI, in particular, the channels are similar, thus, we may suppose that the features found on FER would apply for MFI substances as well. In situ spectra were obtained on a sample of high iron-content ferrisilicate. Various treatments were applied, most characteristic spectra are shown in Fig. 3. Data are presented in Table 2.

Table 2
Mössbauer data obtained from selected spectra of Fe-FER (Si/Fe = 16) recorded after sequential treatments

Treatment/(measurement)	Compound	IS (mm/s)	QS (mm/s)	RI (%)
As-synthesized (300 K)	Fe^{3+}	0.22	–	89
	Fe^{3+}	0.31	0.71	11
As-received/calcined (300 K)	Fe^{3+}	0.29	0.56	26
	Fe^{3+}	0.33	1.43	33
	Fe^{3+}	0.36	0.96	40
620/vac. (300 K)	Fe^{3+}	0.24	1.97	71
	Fe^{3+}	0.27	1.06	14
	Fe^{2+}	0.74	1.06	15
620/H_2 (77 K)	Fe^{3+}	0.34	1.81	16
	Fe^{3+}	0.44	1.29	32
	Fe^{2+}	1.13	2.03	39
	Fe^{2+}	1.43	2.46	12
300 K/air/H_2 (300 K)	Fe^{3+}	0.29	1.58	40
	Fe^{3+}	0.31	0.94	51
	Fe^{2+}	0.86	2.34	4
	Fe^{2+}	1.31	2.44	4
620 K/vac. (300 K)	Fe^{3+}	0.23	1.96	53
	Fe^{3+}	0.30	1.45	25
	Fe^{2+}	1.00	0.80	5
	Fe^{2+}	1.04	1.82	16

In parentheses, the temperature of measurement is shown. IS: isomer shift, relative to metallic alpha-iron; QS: quadrupole splitting; RI: spectral contribution (relative intensity).

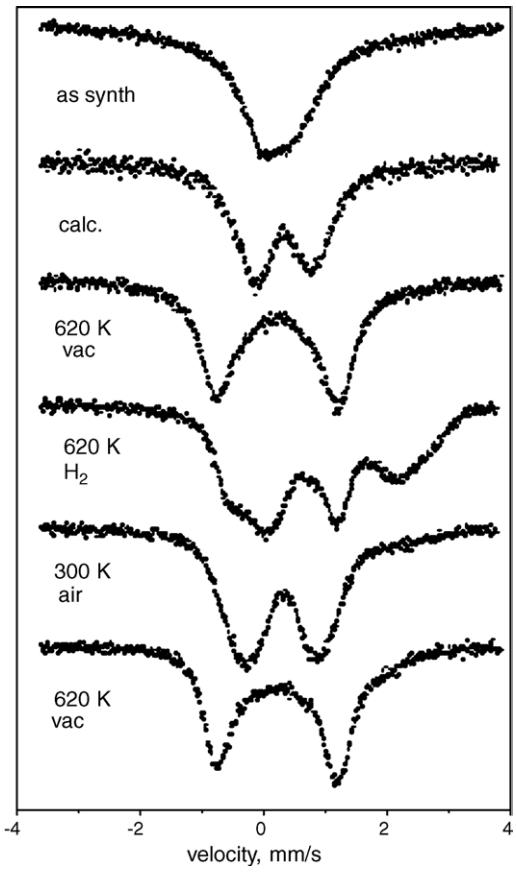

Fig. 3. Sequential in situ Mössbauer spectra recorded on the Fe-FER sample (Si/Fe = 16) in a series of treatments (starting at the top with the as-synthesized sample).

The spectrum of as-synthesized sample exhibits a broad line—the environment of iron is symmetric, since the template molecules are still present in the sample. The Fe^{3+} doublets are more distinguishable in the sample after calcination and conversion to H^+ form after NH_4^+ exchange. Removal of the adsorbed water results in the appearance of the signal of framework substituted iron with H^+ compensation in 71% spectral contribution (Bronsted acidic $(Si–O)_3 \equiv Fe(OH)–Si$ sites; IS = 0.24, QS = 1.97 mm/s). Autoreduction, i.e. formation of Fe^{2+} due to removal from the framework, is also detected for ca. one-sixth of iron. The intentional reduction, treatment in hydrogen at 620 K, significantly reduces the amount of $(Si–O)_3 \equiv Fe(OH)–Si$ FW component, with simulataneous appearance of a pair of novel Fe^{3+} ($IS_{300\ K} \sim 0.30$, QS = 1.29 mm/s) and Fe^{2+} components ($IS_{300\ K} \sim 1.0$, QS = 2.03 mm/s). It is worth to note that the spectral contribution of these components are similar, ca. one-third part of each. With regard to the similar proportion and the novel appearance it may be proposed that this pair of data characterizes a dinuclear, $Fe^{3+}_{FW}–O–Fe^{2+}_{EFW}$ component. Formation of these pairs assumes migration of neutral components and charge transfer in an extent. For example, the majority of Bronsted acidic $(Si–O)_3 \equiv Fe(OH)–Si$ groups might be converted to $Fe^{3+}_{FW}–O–Fe^{2+}_{EFW}$ pairs in a $Fe^{(2+)}O + (Si–O)_3 \equiv Fe^{(3+)}(OH^+)–Si \rightarrow (Si–O)_3 \equiv Fe^{(3+)}(O)[Fe^{(2+)}(OH)]^+–Si$ process (similar charge transfer from Bronsted acidic H^+ to neutral oxidic components of iron has already been proposed—although at higher temperatures [22]). A slight oxidation and an evacuation restores a higher percentage for the Bronsted acidic protonated component, i.e. a part of the dinuclear centre is probably decomposed in an opposite process and neutral FeO(OH) may leave the vicinity of FW iron:

$$(Si–O)_3 \equiv Fe^{(3+)}(O)[Fe^{(3+)}(OH)_2]^+–Si \rightarrow (Si–O)_3 \equiv Fe^{(3+)}(OH^+)–Si + Fe^{(3+)}O(OH).$$

It might be mentioned that in this interpretation the $Fe^{3+} \leftrightarrow Fe^{2+}$ redox cycle is restricted to proceed only on the EFW part of the dinuclear component, in a certain contrast to the explanation presented in our earlier report [12], where the redox cycle was supposed to proceed on both, FW and EFW types of iron. Thus, dynamic formation and decomposition of dinuclear centres can be proposed in the evacuation–reduction–oxidation–evacuation cycle, combined with charge transfer and migration of neutral components.

3.3. Mesoporous samples

Stabilization of iron is related to local crystallinity, and hence, it may depend also on the host, whether it is a strictly crystalline microporous system with 3D crystallinity or a mesoporous one with partly amorphous pore walls. The extent of ordering may also depend on the synthesis as for the latter case.

Two MCM-41 samples of different preparation are compared henceforth. The first sample (Si/Fe ∼ 100) was synthesized in a hydrothermal process at 373 K, whereas the second one in a more rapid process at 300 K in a media containing ethanol additionally.

The morphology of the products is distinctly different; the shape of particles prepared by the first method is irregular, whereas the synthesis in ethanolic media results mostly in spherical particles of 150–350 nm diameter. XRD patterns exhibit the characteristic feature: high intensity d_{100} reflexion in the $2\theta < 3^\circ$ region, with a pair of low intensity peaks centred around $2\theta \sim 5^\circ$. A complementary analysis of data reveal that the pore walls are thicker with ca. 20% in the particles of the second sample (Table 3; [23]). It is worth mentioning that the 0.7 nm wall thickness is considered as the lower limit of stable structures [24], and the WTH (2) value for the sample prepared by the first method does not even attain this threshold value.

3.4. MCM-41 (Si/Fe ∼ 100, hydrothermal synthesis)

Selected spectra are shown in Fig. 4, the extracted data are shown in Table 4.

Evacuation results in the appearance of an Fe^{3+} component with large QS, however, the value is slightly less (1.68 mm/s) than found in microporous MFI analogues. It should also be mentioned that this sample hardly exhibits Bronsted acidity—as revealed by pyridine chemisorption measurements [23], thus, this component can probably be attributed to distorted trigonal

Table 3
Comparison of structural properties of MCM-41-s of different preparations

Synthesis	Si/Fe	d_{100} (nm)	a_0 (nm)	Φ_{BJH} (nm)	WTH (1) (nm)	V_p (cm^3/g)	W_d (nm)	WTH (2) (nm)
Hydroth (373 K)	100	3.38	3.90	2.43	1.47	0.79	3.27	0.63
Ethanol (300 K)	20	3.47	4.01	2.31	1.70	0.62	3.20	0.81

d_{100}: Distance determined from 100 reflexions in the XRD, a_0: cell constant ($2d_{100}/\sqrt{3}$), Φ_{BJH}: pore diameter determined from sorption isotherms by method of Barett–Joyner–Halenda, WTH (1): wall thickness ($a_0 - \Phi_{BJH}$), V_p: pore volume, W_d: diameter of primary mesopores by method of Kruk and Jaroniec, WTH (2): wall thickness, calculated from the diameter of primary mesopores ($a_0 - W_d$).

Fe^{3+} in the pore wall. The other characteristic feature is the appearance of Fe^{2+} in high proportion (30% RI). This high percentage is probably not related primarily to the autoreduction (removal of framework tetra-coordinated iron), it can be attributed rather to simple reduction taking also into account the presence of –OH in the amorphous pore wall in high portion, e.g.:

$$2Si{-}O{-}Fe^{(3+)}(OH)_2 \rightarrow 2Si{-}O{-}Fe^{(2+)}(OH) + \tfrac{1}{2}O_2 + H_2O.$$

The 670 K/CO treatment was applied to test whether Fe–O–Fe pairs exist (presuming that CO may extract oxygen from these pairs by simultaneous $Fe^{3+} \rightarrow Fe^{2+}$ reduction of the two adjacent irons). A reduction in a modest extent is detected, however, almost ca. one-half of iron preserves still the Fe^{3+} oxidation state. In contrast, a hydrogen treatment at the same temperature converts almost all Fe^{3+} to Fe^{2+} (only 5% is retained in ferric state). It is worth to note that novel, distorted Fe^{2+} coordination (QS = 0.83 and 1.10 mm/s) appear, which have not been detected in microporous structures. These profound changes can probably be attributed to formation of hydroxyl groups and bridges in the partially amorphous pore walls. Further, participation of $(H_2)^+$ ions in reduction [25] and propagation via hydrogen bridges can also be proposed [13]. The reduction in hydrogen rearranges the structure in an extent, after calcination and repeated reduction with CO larger portion of Fe^{3+} can be reduced (78% RI) than in the first CO treatment (56%). The spectrum similar to the first CO treatment can rather be restored by evacuation of the sample (after the second CO treatment).

In short, the MCM-41 sample exhibited distinct differences in comparison with the microporous MFI analogues:

- the Bronsted acidity (and presence of distorted tetra-coordinated FW iron component) is not characteristic;
- in the $Fe^{3+} \leftrightarrow Fe^{2+}$ reversible redox process almost all the iron may participate;
- novel, distorted Fe^{2+} coordination appear upon hydrogen treatment.

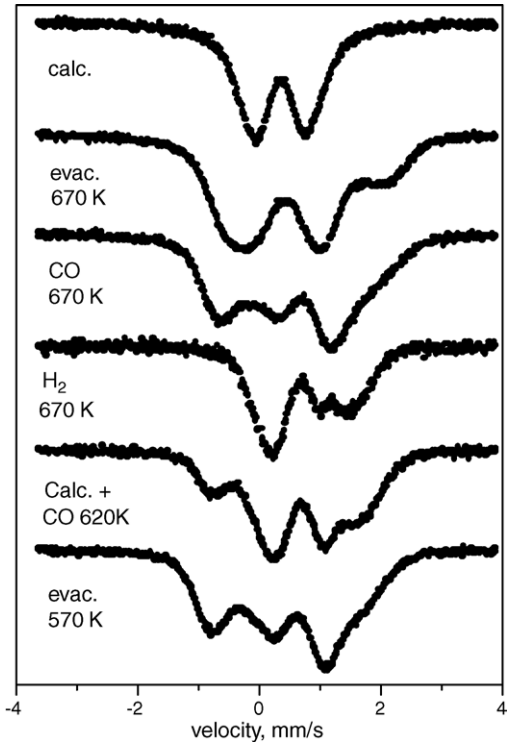

Fig. 4. Sequential in situ Mössbauer spectra recorded on the Fe-MCM-41 sample (Si/Fe ∼ 100) prepared by hydrothermal synthesis (the series of treatments starts at the top with the calcined sample).

Table 4
Mössbauer data obtained from selected spectra of Fe-MCM-41 of hydrothermal synthesis (Si/Fe ∼ 100) recorded after sequential treatments

Treatment/(measurement)	Compound	IS (mm/s)	QS (mm/s)	RI (%)
As-synthesized/	Fe^{3+}	0.35	0.68	40
calcined (300 K)	Fe^{3+}	0.37	1.13	60
Evacuation/670 K	Fe^{3+}	0.28	1.68	44
(300 K)	Fe^{3+}	0.34	1.04	27
	Fe^{2+}	1.07	2.03	30
CO/670 K (300 K)	Fe^{3+}	0.23	1.76	45
	Fe^{2+}	0.87	1.03	24
	Fe^{2+}	0.92	1.97	32
H_2/670 K (530 K)	Fe^{3+}	0.12	0.57	5
	Fe^{2+}	0.59	0.83	32
	Fe^{2+}	0.86	1.10	33
	Fe^{2+}	0.87	1.70	30
1. Calcined/670 K	Fe^{3+}	0.38	2.30	22
2. CO/620 K (450 K)	Fe^{2+}	0.60	1.00	49
	Fe^{2+}	0.71	0.61	7
	Fe^{2+}	1.06	1.56	22
Vac./670 K (570 K)	Fe^{3+}	0.13	1.78	48
	Fe^{2+}	0.78	0.91	18
	Fe^{2+}	0.87	1.70	34

In parentheses, the temperature of measurement is shown. IS: isomer shift, relative to metallic alpha-iron; QS: quadrupole splitting; RI: spectral contribution (relative intensity).

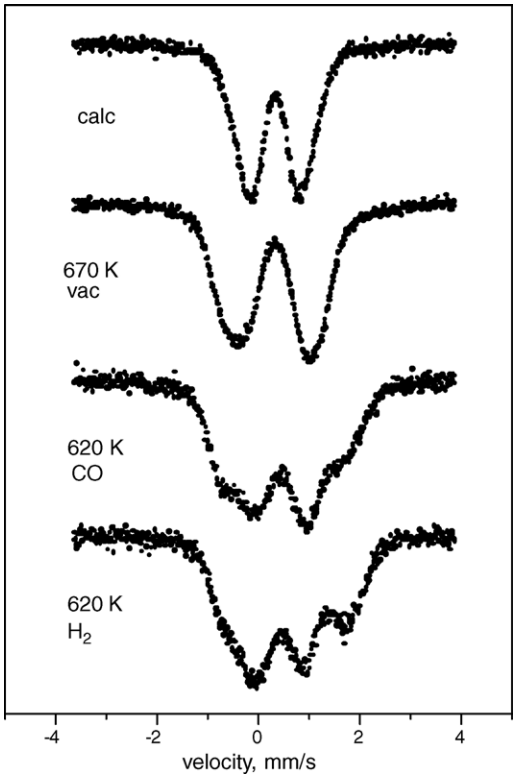

Fig. 5. Sequential in situ Mössbauer spectra recorded on the Fe-MCM-41 sample (Si/Fe = 20) synthesized from TEOS silica source in partly ethanolic media (the series of treatments starts at the top with the calcined sample).

All the mentioned differences can easily be correlated with the partially amorphous structure of the pore wall, and with abundant presence of –OH groups in the pore walls.

In other words, the assignation of FW and EFW positions is not applicable for the mesoporous systems, since FW sites are not defined in strict crystallographic clarity.

3.5. MCM-41 (Si/Fe = 20, synthesis in ethanolic media)

Particles of this sample are mostly of spherical shape, and they have thicker pore walls then the sample of hydrothermal synthesis. The in situ Mössbauer spectra are also different in some aspects (see Fig. 5; Table 5).

In contrast to the previous MCM-41 sample, evacuation did not result in noticeable formation of Fe^{2+} species, the spectrum is characteristic of various Fe^{3+} species. The effects of reduction with CO are more similar—the $Fe^{3+} \rightarrow Fe^{2+}$ reduction is partial, ca. two-thirds of iron retain the Fe^{3+} state. The stability of structure is even more expressed in hydrogen reduction—ca. 60% of iron retain the Fe^{3+} state in this treatment. It also worth to refer to the corresponding pyridine chemisorption data; the signal of pyridinium ion in IR spectra is well distinguishable at 1556 cm^{-1}, however its intensity is rather small in comparison to those of the bands characterizing pyridine sorbed on Lewis centres [14]. Further, it can also be noticed that upon hydrogen reduction Fe^{3+} (lower QS: 1.06 mm/s) and and Fe^{2+} species are present in ca. 1/3:1/3 proportions, thus, similarly to the FER case, presence of dinuclear species might also be supposed. However, the QS values are smaller than found in the FER sample, indicating that the coordination is different. This is apparent since the pore walls of mesoporous structure may host iron in more variety of coordinations than the micrporous MFI analogue, thus the FW versus EFW distinction probably does not clearly apply.

Table 5
Selected Mössbauer spectra of Fe-MCM-41 (Si/Fe = 20) synthesized using TEOS in partially ethanolic media

Treatment/(measurement)	Compound	IS (mm/s)	QS (mm/s)	RI (%)
As-synthesized/	Fe^{3+}	0.34	0.79	38
calcined (300 K)	Fe^{3+}	0.34	1.30	62
Evacuation/660	Fe^{3+}	0.28	2.02	39
K (300 K)	Fe^{3+}	0.32	1.42	39
	Fe^{3+}	0.35	0.90	22
CO/620 K (490 K)	Fe^{3+}	0.17	1.79	31
	Fe^{3+}	0.27	1.07	34
	Fe^{2+}	0.87	1.41	23
	Fe^{2+}	0.97	1.91	12
H_2/620 K (490 K)	Fe^{3+}	0.17	1.72	20
	Fe^{3+}	0.25	1.06	39
	Fe^{2+}	0.91	1.53	32
	Fe^{2+}	0.97	2.05	9

In parentheses, the temperature of measurement is shown. IS: isomer shift, relative to metallic alpha-iron; QS: quadrupole splitting; RI: spectral contribution (relative intensity).

The differences are apparent when comparing the behaviour of the two MCM-41-s prepared by different syntheses. Larger part of iron can be exposed to redox $Fe^{2+} \leftrightarrow Fe^{3+}$ changes and structural rearrangements in the in the sample of hydrothermal synthesis. This can probably be attributed to the thin pore walls (as was mentioned earlier, the wall thickness in this sample hardly reaches the expected stability limit). A ca. 20% increase in the wall thickness results in more stable structure incorporating iron in Fe^{3+} state in larger proportions.

4. Conclusions

Iron was incorporated during syntheses of microporous (MFI analogue) and mesoporous (MCM-41) structures, and stabilization and redox properties of iron have been characterized in these hosts mostly by in situ Mössbauer spectroscopy.

Microporous hosts possess 3D crystallinity—FW and EFW sites could be distinguished upon symmetry of coordination and reducibility. In ZSM-5 of low iron-content (Si/Fe $\sim$ 200) slow relaxation of spins of single separated Fe^{3+} ions is reflected in the 77 K spectra. Further, occurence of Fe^{4+} oxidation state is hypothesized, and reversible processes among Fe^{4+} and Fe^{3+}, as well as Fe^{3+} and Fe^{2+} are demonstrated. In FER with higher Fe content (Si/Fe = 16) dynamic formation and decomposition of dinulear Fe_{FW}–O–Fe_{EFW} pairs is suggested with simultaneous charge transfer and migration of neutral iron species.

The crystal structure of mesoporous hosts is less expressed, their pore walls are partly amorphous and contain –OH groups in a large extent. The MCM-41 sample (Si/Fe $\sim$ 100) made by hydrothermal route is composed from thin pore walls. In correspondence, almost all iron may participate in reversible

$Fe^{3+} \leftrightarrow Fe^{2+}$ processes, novel Fe^{2+} coordination (not present in microporous hosts) can be detected, and participation of –OH groups in the redox processes can be suggested. A slight variation in the synthesis (in ethanolic media and TEOS silica source) may result in formation of more dense and thicker pore walls. In correspondence, smaller part of iron participates in $Fe^{3+} \leftrightarrow Fe^{2+}$ transformations. The partly amorphous character is manifested in stabilization of Fe^{2+} components in distorted coordination.

References

[1] G. Centi, B. Wichterlová, A.T. Bell (Eds.), Catalysis by Unique Metal Ion Structures in Solid Matrices, NATO Science Series II, vol. 13, Kluwer, 2001.
[2] F. Kapteijn, J. Rodriguez-Mirasol, J.A. Moulijn, Appl. Catal. B Environ. 9 (1996) 25.
[3] B. Wichterlová, Z. Sobalík, J. Dědeček, Appl. Catal. B Environ. 41 (2003) 97.
[4] M. Stockenhuber, M.J. Hudson, R.W. Joyner, J. Phys. Chem. B 104 (2000) 3370.
[5] S. Schacht, M. Janicke, F. Schüth, Microporous Mesoporous Mater. 22 (1998) 485.
[6] R. Burns, Hyperfine Interactions 91 (1994) 739.
[7] A. Meagher, V. Nair, R. Szostak, Zeolites 8 (1988) 3.
[8] K. Lázár, G. Borbély, H. Beyer, Zeolites 11 (1991) 214.
[9] J.B. Taboada, A.R. Overweg, M.W.J. Crajé, I.W.C.E. Arends, G. Mul, A.M. van der Kraan, Microporous Mesoporous Mater. 75 (2004) 237.
[10] K.A. Dubkov, N.S. Ovanesyan, A.A. Shteinman, E.V. Starokon, G.I. Panov, J. Catal. 207 (2002) 341.
[11] P. Fejes, I. Kiricsi, K. Lázár, I. Marsi, A. Rockenbauer, L. Korecz, J.B. Nagy, R. Aiello, F. Testa, Appl. Catal. A Gen. 242 (2003) 247.
[12] K. Lázár, G. Lejeune, R.K. Ahedi, S.S. Shevade, A.N. Kotasthane, J. Phys. Chem. B 102 (1998) 4865.
[13] K. Lázár, G. Pál-Borbély, Á. Szegedi, H.K. Beyer, Stud. Surf. Sci. Catal. 142 (2002) 1347.
[14] Á. Szegedi, Z. Kónya, D. Méhn, E. Solymár, G. Pál-Borbély, Z.E. Horváth, L.P. Bíró, I. Kiricsi, Appl. Catal. A Gen. 272 (2004) 257.
[15] K. Lázár, K. Matusek, J. Mink, S. Dobos, L. Guczi, A. Vizi-Orosz, L. Markó, W.M. Reiff, J. Catal. 87 (1984) 163.
[16] S. Mørup, in: A. Vértes, D.L. Nagy (Eds.), Mössbauer Spectroscopy of Frozen Solutions, Akadémiai, Budapest, 1990, p. 71.
[17] R. Kumar, S.K. Date, E. Bill, A. Trautwein, Zeolites 11 (1991) 211.
[18] N.N. Greenwood, T.C. Gibb, Mössbauer Spectroscopy, Chapman and Hall Ltd., London, 1971.
[19] J. Jia, Q. Sun, B. Wen, L.X. Chen, W.M.H. Sachtler, Catal. Lett. 82 (2002) 7.
[20] A. Heyden, B. Peters, A.T. Bell, F.J. Keil, J. Phys. Chem. B 109 (2005) 1857.
[21] A.L. Yakovlev, G.M. Zhidomirov, R.A. van Santen, J. Phys. Chem. B 105 (2001) 12297.
[22] Q. Zhu, B.L. Mojet, R.A.J. Janssen, E.J.M. Hensen, J. van Grondelle, P.C.M.M. Magusin, R.A. van Santen, Catal. Lett. 81 (2002) 205.
[23] Á. Szegedi, Theses, Budapest, 2004.
[24] M. Kruk, M. Jaroniec, A. Sayari, J. Phys. Chem. B 101 (1997) 2499.
[25] O.E. Lebedeva, W.M.H. Sachtler, J. Catal. 191 (2000) 364.